Membrane and Water Treatment, *Vol. 15, No. 2 (2024) 67-78*
https://doi.org/10.12989/mwt.2024.15.2.067

Application of nickel hexacyanoferrate and manganese dioxide-polyacrylonitrile (NM–PAN) for the removal of Co^{2+}, Sr^{2+} and Cs^{+} from radioactive wastewater

Md Abdullah Al Masud and Won Sik Shin*

School of Architecture, Civil, Environmental, and Energy Engineering, Kyungpook National University, 80 Daehakro, Bukgu, Daegu 41566, Republic of Korea

(Received August 11, 2023, Revised May 27, 2024, Accepted June 24, 2024)

Abstract. In this study, a nickel hexacyanoferrate and manganese dioxide-polyacrylonitrile (NM–PAN) composite was synthesized and used for the sorptive removal of Co^{2+}, Sr^{2+}, and Cs^{+} in radioactive laundry wastewater. Single- and multi-solute competitive sorptions onto NM–PAN were investigated. The Freundlich (Fr), Langmuir (Lang), Kargi–Ozmıhci (K–O), Koble–Corrigan (K–C), and Langmuir–Freundlich (Lang–Fr) models satisfactorily predicted all the single sorption data. The sorption isotherms were nonlinearly favorable (Freundlich coefficient, N_F = 0.385–0.426). Cs^{+} has the highest maximum sorption capacity (q_{mL} = 0.855 mmol g^{-1}) for NM–PAN compared to Co^{2+} and Sr^{2+}, wherein the primary mechanism was the physical process (mainly ion-exchange). The competition between the metal ions in the binary and ternary systems reduced the respective sorption capacities. Binary and ternary sorption models, such as the ideal adsorbed solution theory (IAST) model coupled with single sorption models of IAST–Fr, IAST–K–O, IAST–K–C and IAST–Lang–Fr, were fitted to the experimental data; among these, the IAST–Freundlich model showed the most satisfactory prediction for the binary and ternary systems. The presence of cationic surfactants highly affected the sorption on NM–PAN due to the increase in distribution coefficients (K_d) of Co^{2+} and Cs^{+}.

Keywords: IAST; multi-solute sorption; NM–PAN; radioactive; wastewater

1. Introduction

Radioactive laundry wastewater is generated from facilities that handle radioactive materials, such as nuclear power plants, research laboratories, and medical centers (Kadadou *et al.* 2023). This wastewater contains various radioactive contaminants, including cobalt (^{60}Co), strontium (^{90}Sr), and cesium (^{137}Cs), which pose significant environmental and health risks if not properly treated before discharge (Babatunde and Zhao 2010, Oh *et al.* 2015). Among those, Cs was the most hazardous and abundant radioactive element produced at power plants owing to its long half-life around 30 years (Rauwel and Rauwel, 2019). Cs can be easily absorbed by aquatic organisms due to its similar physicochemical properties to potassium (K) (Nilchi *et al*. 2011). To humans, Cs can easily enter and be distributed throughout the body, especially in muscles and bones, because its physicochemical properties are like those of K and Na, leading to genetic mutation and cancer (Le and Cho 2021). To the environment, Rumynin and Nikulenkov (2016), reported that ^{60}Co, ^{90}Sr, and ^{137}Cs were sorbed onto the sediment at the nuclear reactor and in radioactive waste disposal areas (Rumynin and Nikulenkov, 2016). Since the number of nuclear power plant catastrophes, including the Three Mile Island accident in the USA in 1979, Chernobyl in the Ukraine in 1986, and the Fukushima disaster in Japan in 2011, the management of radioactive wastes has gained importance (Rauwel and Rauwel 2019).

The treatment of low-level liquid radioactive wastes has been proposed to use a variety of methods, including thermal treatment, precipitation, extraction, membrane, adsorption, and ion exchange (Liu *et al.* 2023, Sopapan *et al.* 2023, Min *et al.* 2023). However, an economically feasible removal technique is also necessary to minimize the operational cost of radioactive waste removal (Gonzalez de Vicente *et al.* 2022). Sorption is the most favorable technique to remove radioactive waste elements from water due to its simplicity, efficiency, and economic feasibility (Ebner *et al.* 2001). Generally, the sorption of radioactive waste elements occurs through ion exchange (Ebner *et al.* 2001, Oh *et al.* 2015, Park *et al.* 2010). In our previous studies, we successfully achieved Co^{2+}, Sr^{2+}, and Cs^{+} sorption in the aqueous solution using natural and synthesized sorbents, such as fishbone (Park *et al.* 2013). Removal of cobalt and strontium from groundwater by sorption onto fishbone, synthetic hydroxyapatite nano-particles (Ma *et al.* 2010), ammonium molybdophosphate–polyacrylonitrile (AMP–PAN) (Park *et al.* 2010), manganese and iron oxide-coated montmorillonite (Park *et al.* 2013), and hydrous manganese oxide–polyacrylonitrile (HMO–PAN) (Oh *et al.* 2015), through ion exchange. However, the effect of a multi-solute system of radioactive waste on the sorbent's sorption capacity has rarely been investigated. Moreover, it is essential to continuously improve the

*Corresponding author, Ph.D.,
E-mail: wshin@knu.ac.kr

ISSN: 2005-8624 (Print), 2092-7037 (Online)

removal efficiency of radioactive wastes. In present study, NM was modified with PAN to improve its sorption efficiency, selectivity, and chemical resistance. NM acts as the ion exchanger (active component), whereas PAN is an inert binder that reduces the solubility of the active component (Nilchi *et al.* 2011).

This study aimed to investigate the applicability of NM–PAN as a sorbent for removing radioactive Cs^+, Sr^{2+}, and Co^{2+} in the radioactive laundry wastewater. Sorption using NM–PAN is a promising technique for removing radioactive materials from water. The sorption in single and multi-component systems is crucial for determining the competitive effects of Cs^+, Sr^{2+}, and Co^{2+} on NM–PAN. To analyze the single sorption data, the Freundlich, Langmuir, Kargi–Ozmıhci (K–O), Koble–Corrigan (K–C), and Langmuir–Freundlich models were used. To the best of our knowledge, this is the first study attempting to apply binary and ternary sorption models, such as the ideal adsorbed solution theory (IAST) model coupled with single sorption models of Freundlich (IAST–Freundlich), Langmuir (IAST–Langmuir), and Langmuir–Freundlich (IAST–Langmuir–Freundlich), to evaluate the binary and ternary sorption characteristics of divalent Co^{2+} and Sr^{2+} and monovalent Cs^+ for NM–PAN. We also investigated the effects of the anionic, cationic, and non-ionic surfactants on the distribution coefficients (K_d) of Cs^+, Sr^{2+}, and Co^{2+}. The result of this study can predict the effect of binary and ternary systems on the sorption of Cs^+, Sr^{2+}, and Co^{2+} onto NM–PAN.

The successful application of NM–PAN composites in treating radioactive laundry wastewater could offer a cost-effective and environmentally friendly solution for the nuclear industry and other facilities dealing with radioactive materials. This research seeks to contribute valuable insights to the field of radioactive wastewater treatment and advance the development of sustainable technologies for safeguarding the environment and public health.

2. Materials and methods

2.1 Chemicals

Manganese(II) nitrate ($Mn(NO_3)_2{\cdot}4H_2O$, Aldrich Chemical Co., ≥ 97.0%), sodium permanganate ($NaMnO_4{\cdot}H_2O$, Aldrich Chemical Co., > 97%) and sodium hydroxide (NaOH, Duksan Chemical Co., > 97%) were used to synthesize hydrous manganese oxide (HMO). Potassium ferrocyanide ($K_4Fe(CN)_6{\cdot}3H_2O$, Sigma-Aldrich, 98.5-102.0%), nickel nitrate ($Ni(NO_3)_2{\cdot}6H_2O$, Yakuri Chemical Co., < 98%) were used to synthesize potassium-nickel hexacyanoferrate(II) (KNiFC). The mixture (1:1 mass ratio) of HMO and KNiFC, dimethyl sulfoxide (DMSO, $(CH_3)_2SO$, 99% +, Junsei Chemical Co., Ltd., Japan) and PAN (polyacrylonitrile, M.W. = 150,000, Sigma-Aldrich) were used to synthesize NM–PAN. Cobalt nitrate ($Co(NO_3)_2{\cdot}6H_2O$, ≥ 98%), $Sr(NO_3)_2$ (99.0% ≥) and $CsNO_3$ (99%) were purchased from Sigma-Aldrich Chemical Co. (Seoul, Korea). MES buffer (2-[N-morpholino] ethanesulfonic acid hydrate, Acros Organics, USA) was used to adjust solution pH in sorption experiments. Na^+ and Ca^{2+} were introduced as $NaNO_3$ (Sigma-Aldrich Chemical Co., Seoul, Korea) and $Ca(NO_3)_2{\cdot}4H_2O$ (Sigma-Aldrich Chemical Co., Seoul, Korea). Non-ionic surfactants, Tween-80 (Reidal-de-Haen, Germany) and Triton X-100 (Aldrich, Chemical Co., Korea), anionic surfactants, SOBS (sodium 4-n-octylbenzenesulfonate, $C_{14}H_{21}NaO_3S$, TCI, Japan) and SDBS (sodium dodecylbenzenesulfonate, $C_{18}H_{29}NaO_3S$, Aldrich Chemical Co., Korea), and cationic surfactants, OTMA (n-octyltrimethlammonium chloride, $C_{11}H_{26}ClN$, TCI Co., Ltd., Japan) and HDTMA (hexadecyltrimethyl-ammonium chloride, $C_{19}H_{42}NCl$, Sigma-Aldrich Chemical Co., Seoul, Korea) were used as model surfactants. All reagents were of analytical grade and were used without further purification.

2.2 Sorbent preparation

The NM–PAN (nickel hexacyanoferrate and manganese dioxide-polyacrylonitrile) bead was synthesized by slightly modifying the procedure reported by Moon *et al.* (2000) and Park *et al.* (2010). The nickel hexacyanoferrate (KNiFC) *(*Ismail *et al.* 1999) and manganese dioxide (HMO) (Oh *et al.* 2015) were mixed by 1:1 mass ratio to prepare NM mixture. The synthesized NM mixture was used to prepare the inorganic-organic active ion exchangers. Briefly, 20 g of NM mixture and 0.8 g of Tween-80 were combined with 100 mL of dimethyl sulfoxide (DMSO). After stirring the solution for 1 hour at 50 °C and 250 rpm. Then, 8 g of PAN was added to this solution and then stirred using a mechanical agitator for 5 hours at 50 °C and 250 rpm to obtain a homogeneous solution of the composite dope. The NM–PAN beads were washed three times with DI water and then dried in an oven for 24 h at 60 °C. The synthesized NM–PAN was composed of 70 wt.% of NM loaded on a PAN support, which is the optimum ratio to form its sphere shape (Moon *et al.* 2000)

2.3 Sorption experiments

For single-solute sorption experiments, the stock solutions of Co^{2+}, Sr^{2+}, and Cs^+ were prepared by dissolving $Co(NO_3)_2{\cdot}6H_2O$, $Sr(NO_3)_2$ and $CsNO_3$, respectively in DI water. For the sorption isotherm at pH 5.0, MES buffer was used, and for the effect of the initial solution pH, 0.1 N HNO_3 and 0.1 N NaOH were used to adjust the pH. The solution pH was measured with a pH meter (Thermo Orion, model 720A+, USA). Sorption experiments were conducted at 25 °C using a 15 mL conical centrifuge tube (polyethylene, SPL Labware, Korea). 0.5 g of NM–PAN for Co^{2+} and Sr^{2+} sorptions and 0.2 g of NM–PAN for Cs^+ sorption, respectively, were transferred into the tube before the addition of heavy metal solution. To obtain sorption isotherms, different initial concentrations (1, 2, 5, 10, 15, and 20 or 30 mM) of each metal solution were used.

The mixture was then placed on a rotary shaker and shaken for 24 hours at 200 rpm. After mixing, the tubes were centrifuged for 20 min at 3000 rpm, and the filtrate was filtered through a 0.2 μm syringe filter (Whatman, cellulose nitrate membrane filter, ϕ = 25 mm). The metal ion concentration in the filtrate was analyzed by inductively coupled plasma optical emission spectrometry (ICP-OES,

Optima 2100 DV, Perkin-Elmer Co., USA). The concentrations of Cs^+ were analyzed using standard addition methods [16]. The solid phase equilibrium concentrations were calculated by assuming all concentration changes in the solution phase result from sorption onto the solid phase. All experiments were run in duplicate.

The sorbed amount of metal ion, q (mmol g^{-1}), was calculated using difference between initial and equilibrium metal concentrations.

$$q = \frac{(C_0 - C)V}{W} \quad (1)$$

where C_0 (mmol L^{-1}) and C (mmol L^{-1}) are initial and equilibrium metal ion concentrations in solution, respectively and V (L) is the volume of the solution and W (g) is the weight of sorbent.

Bi-solute systems (Co^{2+}/Sr^{2+}, Co^{2+}/Cs^+ and Sr^{2+}/Cs^+) were prepared by mixing each metal solution of the same molar concentration in a 1:1 volume ratio for each solute. Bi-solute competitive sorption experiments were conducted in the same manner as were in the single-solute sorption experiments. The equilibrium concentrations in the mixture were also determined using the ICP-OES. Tri-solute ($Co^{2+}/Sr^{2+}/Cs^+$) competitive sorption experiments were conducted in the same manner.

2.4 Surfactants

The effects of surfactants on the sorption of Cs^+, Sr^{2+}, and Co^{2+} were investigated by applying initial concentrations of 10 mM to each metal. We used three types of surfactants, namely, SOBS and SDBS as anionic surfactants, OTMA and HDTMA as cationic surfactants, and Triton X-100 and Tween-80 as non-ionic surfactants. The experiments were conducted in the same manner as the single sorption experiments and the K_d value was calculated to evaluate the effects of surfactants (Oh *et al.* 2015).

2.5 Characterization of sorbent

The Brunauer–Emmett–Teller (BET) surface area (A_{BET}) was obtained from N_2 adsorption isotherm using a specific surface area analyzer (Micromeritics, ASAP-2010). The point of zero charge pH_{pzc}) was determined by batch equilibration technique, using 0.1 M KNO_3 as inert background electrolyte (Masud *et al.* 2023b). The chemical composition was revealed by Energy Dispersive Spectroscopy (EDS) analysis (Horiba E-MAX EDS detector). The video microscope (VM, Sometech, SV-35) was used to observe the particle size. The mineral composition of the binders was also investigated using X-Ray Fluorescence (XRF, PW2400, Philips Electronic Instruments, Inc., The Netherlands). The Fourier-transform infrared (FT–IR) spectroscopy absorption spectra were obtained using a PerkinElmer Spectrum GX & Autoimage with the KBr pellet technique (Oh *et al.* 2015).

2.6 Statistical analysis

2.6.1 Sorption models for single system

The Freundlich model was used to fit the single sorption data by considering the heterogeneous sorbent surface (Lee *et al*. 2023):

$$q = K_F C^{N_F} \quad (2)$$

where q (mmol g^{-1}) and C (mmol L^{-1}) are the solid- and aqueous-phase equilibrium concentration, respectively, K_F [(mmol g^{-1})/(mmol L^{-1} N^F)] is the Freundlich sorption coefficient related sorption affinity, and N_F (–) is the Freundlich coefficient related to nonlinearity. $N_F \neq 1$ defines nonlinear sorption (Masud *et al.* 2023b).

The Langmuir model can be used to fit the sorption data when a monolayer sorption occurs on a sorbent surface containing a finite number of binding sites. The Langmuir model is represented as:

$$q = \frac{q_{mL} b_L C}{1 + b_L C} \quad (3)$$

where q_{mL} (mmol g^{-1}) and b_L (L $mmol^{-1}$) are the Langmuir parameters that represent maximum sorption capacity and site energy factor, respectively. The dimensionless constant separation factor (R_L) is useful to represent the essential features of the Langmuir isotherm:

$$R_L = \frac{1}{1 + b_L C_0} \quad (4)$$

where C_0 (mmol L^{-1}) is the initial metal concentration. The R_L values (–) indicate the type of isotherm to be unfavorable ($R_L > 1$), linear ($R_L = 1$), favorable ($0 < R_L < 1$), or irreversible ($R_L = 0$,) (Masud *et al.* 2023a).

Kargi–Ozmıhci proposed the K–O model (Kargi and Ozmıhcı 2004) based on the traditional Freundlich model:

$$q = \frac{q_{m,KO} C^{N_{KO}}}{K + C^{N_{KO}}} \quad (5)$$

where $q_{m,KO}$ is the maximum sorption capacity of the sorbent (mmol g^{-1}), N_{KO} is the cooperative binding constant (–), and K is the saturation constant (mmol L^{-1}). If the $N_{KO} = 1$, the K–O model reduces to Langmuir model. The Koble–Corrigan (K–C) model can be used to predict the single sorption data (Oh *et al.* 2015):

$$q = \frac{q_{m,KC} C^{N_{KC}}}{1 + b_{KC} C^{N_{KC}}} \quad (6)$$

where $q_{m,KC}$ and $b_{L,KC}$ are in mmol g^{-1} and L $mmol^{-1}$, respectively.

The Lang–Fr model can also be used to fit the single sorption data and is defined as (Oh *et al.* 2015):

$$q = \frac{q_{m,LF} (b_L C)^n}{1 + (b_{LF} C)^n} \quad (7)$$

where $q_{m,LF}$ (mmol g^{-1}) and b_{LF} (L $mmol^{-1}$) are the Lang–Fr parameters that represent maximum sorption capacity and site energy factor, respectively. The parameter n indicated the exponent of the Lang–Fr. model.

2.6.2 Sorption models for binary and ternary systems

The IAST proposed by Radke and Prausnitz (Radke and Prausnitz 1972) can be used to predict sorbed-phase

concentrations using aqueous-phase concentrations. A material balance on each solute should be used to fit the binary sorption of Co^{2+}/Sr^{2+}, Co^{2+}/Cs^{+} and Sr^{2+}/Cs^{+} and ternary sorption of $Co^{2+}/Sr^{2+}/Cs^{+}$ onto NM–PAN in this study (Oh *et al.* 2015):

$$\pi = \frac{RT}{A}\int_0^{C_1^*}\frac{q_1}{C_1}dC_1 = \frac{RT}{A}\int_0^{C_2^*}\frac{q_2}{C_2}dC_2 = \cdots = \frac{RT}{A}\int_0^{C_N^*}\frac{q_N}{C_N}dC_N \quad (8)$$

or

$$\pi = \frac{RT}{A}\int_0^{q_1^*}\frac{d\ ln\ C_1}{d\ ln\ q_1}dq_1 = \frac{RT}{A}\int_0^{q_2^*}\frac{d\ ln\ C_2}{d\ ln\ q_2}dq_2 = \cdots = \frac{RT}{A}\int_0^{q_N^*}\frac{d\ ln\ C_N}{d\ ln\ q_N}dq_N \quad (9)$$

where π is the spreading pressure, R is the universal gas constant, T is the temperature at which sorption occurs, A is the interfacial area between the solution and solid sorbent, and N is the total number of solutes. A detailed description for IAST calculations is available elsewhere (Masud and Shin, 2022). The single sorption model parameters were estimated using the commercial software package TableCurve 2D® (Version 5.1, SYSTAT Software, Inc.). The fitness between the model prediction and experimental data for binary and ternary systems was evaluated by the sum of squared errors (SSE) and the root mean square error (RMSE) (Masud *et al.* 2022).

3. Results and discussions

3.1 Characterization of NM–PAN

The physicochemical properties of the NM-PAN, such as the A_{BET}, pore size, and pore volume are presented in Table 1. The A_{BET} and pore volume of NM (296.77 $m^2\ g^{-1}$, 0.278 $cm^3\ g^{-1}$) were higher than those of NM–PAN (175.94 $m^2\ g^{-1}$, 0.242 $cm^3\ g^{-1}$). However, the pore size of NM (10.22 Å) was much smaller than that of NM–PAN (55.19 Å). The pH_{pzc} of NM–PAN was 6.15 (Fig. 1), indicating that it was positively and negatively charged at pH values < 6.15 and > 6.15, respectively.

The morphological structure of the prepared NM–PAN composite was obtained by using scanning video microscopy (Fig. 2). The morphology of the NM–PAN composite was that the internal structure of the granules looked very porous (Fig. 2b), which is consistent with the general characteristics of the K(M)FC composite, where M represents manganese dioxide (Nilchi *et al.* 2011). In addition, the pores of the granules in their inner part were larger than those near the surface (Figs. 2a, b).

In addition to this, energy dispersive spectroscopy (EDS) analysis of the sorbent before and after sorption with Co^{2+}, Sr^{2+}, and Cs^{+} was conducted to understand the changes in elemental compositions (Fig. 3). The sorbent

Table 2 The volatile and total suspended solids concentrations in biofilm formed over membrane surface in MABR on different days of operation

Support	Surface area ($m^2\ g^{-1}$) *a)*	Pore Size (Å) *b)*	Pore volume ($cm^3\ g^{-1}$) *c)*	Support
NM	296.77	10.22	0.278	NM
NM–PAN	175.94	55.19	0.242	NM–PAN

a) Nitrogen adsorption-desorption isotherms (BET) surface area
b) The maximum diameter in BJH adsorption pore size distribution
c) Single point average pore volume

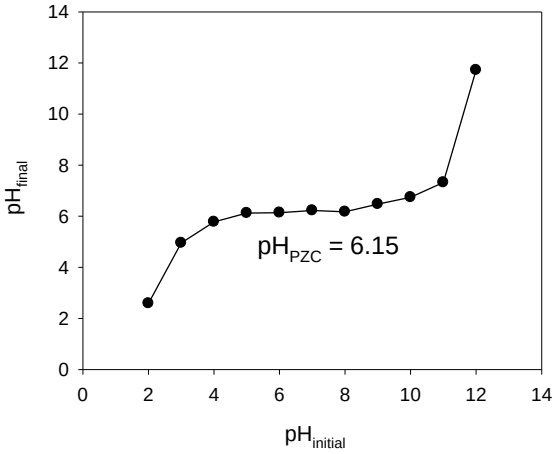

Fig. 1 The point of zero charge (pH_{pzc}) of NM–PAN

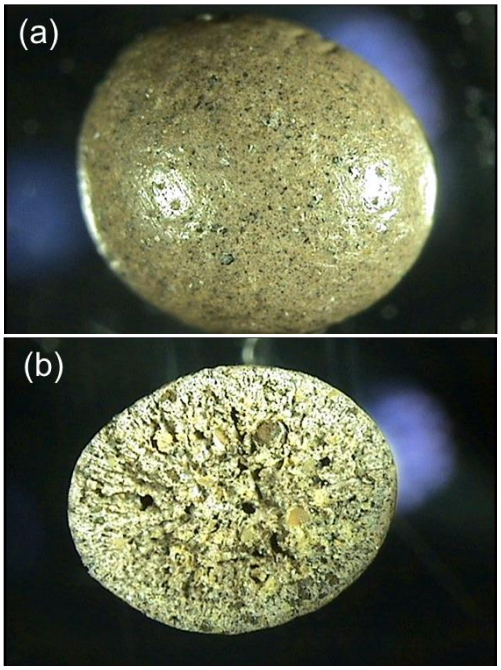

Fig. 2 Video microscopic (VM) images at magnifications of (a) 100× and (b) 200× of NM–PAN

NM–PAN predominately contained C, N, O, and K, as shown in Fig. 3, and Co (Fig. 3b), Sr (Fig. 3c), and Cs (Fig. 3d) peaks occurred after sorption, indicating that the NM–PAN had adsorbed Co^{2+}, Sr^{2+}, and Cs^{+}. As shown in Table 2, XRF analysis also supported the elemental composition of NM-PAN.

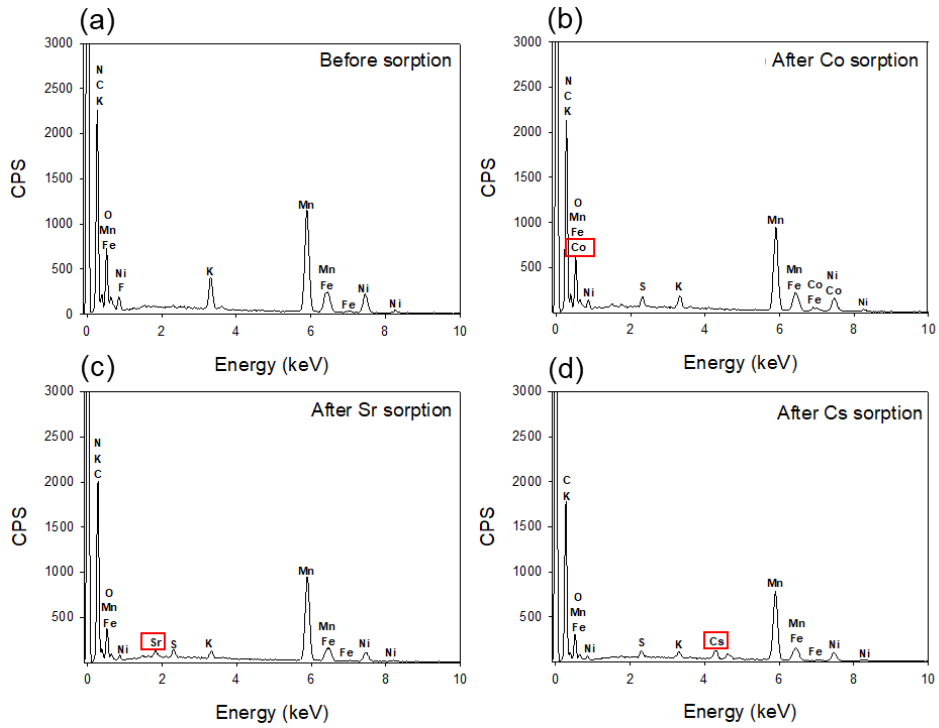

Fig. 3 Energy dispersive spectroscopy (EDS) peaks (a) before sorption, (b) after Co^{2+} sorption, (c) after Sr^{2+} sorption and (d) after Cs^{+} sorption of NM–PAN

Table 2 X-ray fluorescence (XRF) data showing elemental analysis of result of NM and NM-PAN composite

Chemical compounds (%)	NM	NM–PAN
C	20.25	64.07
N	14.31	7.61
O	25.25	10.31
Al	0.11	-
K	7.13	5.66
Fe	5.65	2.14
Ni	8.69	3.67
Mn	15.83	6.54
Na	2.78	-
Total	100	100

In addition to this, energy dispersive spectroscopy (EDS) analysis of the sorbent before and after sorption with Co^{2+}, Sr^{2+}, and Cs^{+} was conducted to understand the changes in elemental compositions (Fig. 3). The sorbent NM–PAN predominately contained C, N, O, and K, as shown in Fig. 3, and Co (Fig. 3b), Sr (Fig. 3c), and Cs (Fig. 3d) peaks occurred after sorption, indicating that the NM–PAN had adsorbed Co^{2+}, Sr^{2+}, and Cs^{+}. As shown in Table 2, XRF analysis also supported the elemental composition of NM-PAN.

The FT–IR spectra of NM–PAN are shown in Fig. 4. Several bands are observed at 3419, 2242, 2096, 1616, 1457 and 594 cm^{-1}. A wide crest was observed in the range of 3600–3000 cm^{-1} that could be attributed to interstitial water and hydroxyl (–OH) groups (Oh *et al.* 2015). The absorption band at 2242 cm^{-1} is due to the nitrile groups in the PAN (Oh *et al.* 2015). Another band is observed at 1616 cm^{-1}, attributed to the vibration of the twist of the water molecule, and not very deep band at 1455 cm^{-1}, probably due to OH groups on manganese, other bands of absorption are observed at 600–400 cm^{-1} and could be assigned to the vibration of Mn–O band (Granados Correa and Jiménez-Becerril, 2004). When Sr^{2+}, Co^{2+} and Cs^{+} were sorbed on the NM–PAN, the IR spectra obtained were changed and became weaker. The band present at 3419 cm^{-1} in NM–PAN was shifted to 3423, 3420 and 3423 cm^{-1} with a high decrease in the intensity after Sr^{2+}, Co^{2+} and Cs^{+} sorption.

3.2 Effect of initial solution pH

The adsorption and precipitation of Sr^{2+}, Co^{2+} and Cs^{+} as a function of initial solution pH was examined over a pH range of 2–12 and the results are presented in Fig. 5. The adsorption of Co^{2+} onto NM–PAN increased with increasing initial solution pH up to 9 and then reached a plateau at pH range of 9–12 (Fig. 5a). The adsorption of Co^{2+} was hindered by the presence of competitive H^{+} as pH decreased, resulting relative low adsorption capacity (0.28 mmol g^{-1}). This may be due to a rapid formation of $CoOH^{+}$ in this pH range and adsorption processes was quickly completed by interaction with negative charge sites by surface complexation. The amounts of Sr^{2+} and Cs^{+} adsorbed onto NM–PAN particles under different initial solution pHs as well as the precipitation are presented in Figs. 5b and 5c, respectively. In the pH range of 2–12, the contribution of precipitation to the total adsorption was not significant in both Sr^{2+} and Cs^{+} cases.

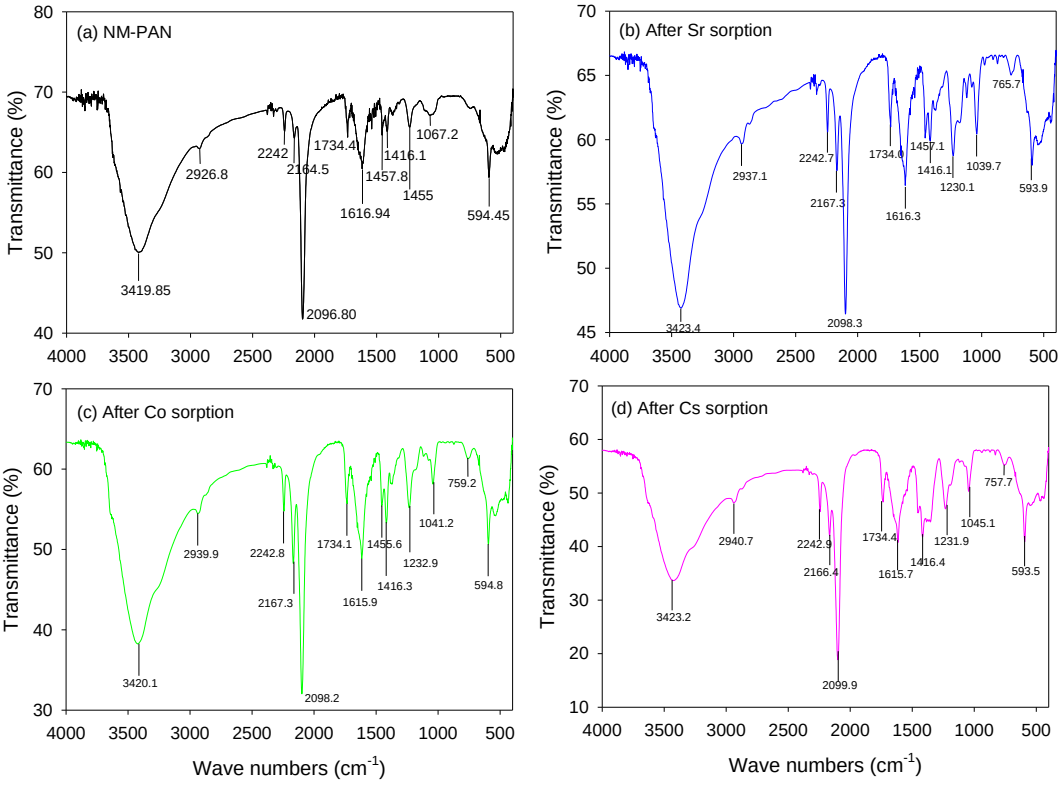

Fig. 4 Fourier-transform infrared spectroscopy (FT-IR) spectra of NM–PAN (a) before and (b–d) after sorption

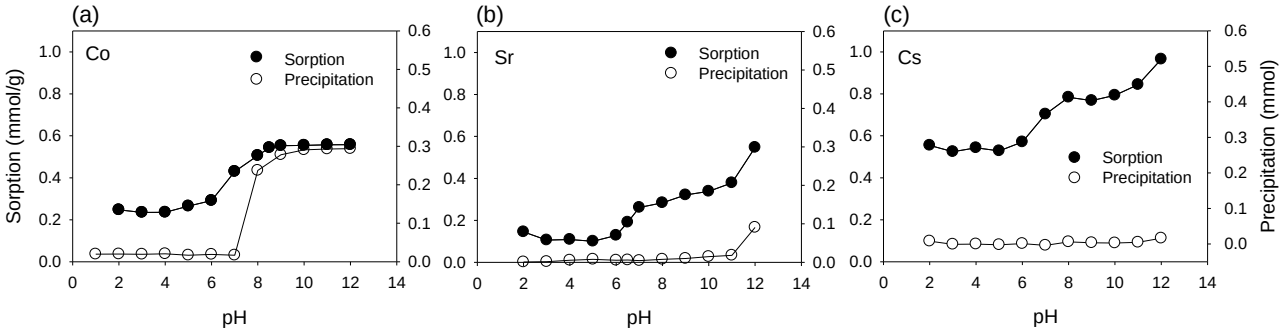

Fig. 5 Effect of solution pH on the sorption of (a) Co, (b) Sr, and (c) Cs ions by NM–PAN

3.3 Single-Solute sorption

The single sorption isotherms of Cs^+, Sr^{2+}, and Co^{2+} onto NM–PAN are shown in Fig. 6. The Freundlich (Fr), Langmuir (Lang), Kargi–Ozmihci (K–O), Koble–Corrigan (K–C) and Langmuir–Freundlich (Lang–Fr) model parameters are summarized in Table 3. The experimental data fitted well with all models (Fr: $0.977 < R^2 < 0.991$, Lang: $0.958 < R^2 < 0.979$, K–O: $0.980 < R^2 < 0.997$, K–C: $0.980 < R^2 < 0.997$, and Lang–Fr: $0.990 < R^2 < 0.994$). For the Freundlich model, all sorption isotherms were nonlinear and favorable physical sorption (Eren *et al.* 2009), as indicated by the N_F values of the Fr model (0.385–0.426), as shown in Table 3. The K_F value was in the following order: $Cs^+ >> Co^{2+} > Sr^{2+}$, indicating that the affinity of NM–PAN was the highest toward monovalent Cs^+ compared to those toward divalent Co^{2+} and Sr^{2+}. Park *et al.* (2010) reported that the Cs^+ sorption onto AMP–PAN fitted well with the Langmuir model, indicating homogenous adsorption on the AMP monolayer. The q_{mL} value in the NM–PAN was in the following order: Cs^+ (0.855 mmol g^{-1}) >> Co^{2+} (0.312 mmol g^{-1}) > Sr^{2+} (0.177 mmol g^{-1}). In the previous study of Co^{2+}, Cs^+, and Sr^{2+} sorption onto HMO–PAN, the q_{mL} values were as follows: Co^{2+} (0.573 mmol g^{-1}) > Cs^+ (0.551 mmol g^{-1}) > Sr^{2+} (0.310 mmol g^{-1}) (Oh *et al.* 2015), indicating that the HMO–PAN sorbed that Co^{2+} more than Cs^+ and Sr^{2+}. This comparison indicated that the NM–PAN was preferable than the HMO–PAN to sorb Cs^+, the most hazardous and abundant radioactive element in the power plant wastewater. The $q_{m,KO}$, $q_{m,KC}$, and $q_{m,LF}$ values according to the KC, KO and Lang–Fr models were also in the following order: $Cs^+ >> Co^{2+} > Sr^{2+}$. These results showed that the sorption capacity of Cs^+ onto NM–PAN was much higher than those Co^{2+} and Sr^{2+}.

Therefore, in this study, the contribution of ion exchange was examined by measuring the desorbed amounts of K^+

Table 3 Freundlich, Langmuir, Kargi–Ozmıhci, Koble–Corrigan, and Langmuir–Freundlich model parameters for the single sorption of Co^{2+}, Sr^{2+} and Cs^{+} at pH 5

Freundlich (Fr) model					
Solute	K_F [(mmol g^{-1})/(mmol L^{-1})N^F]	N_F (–)	R^2	SSE	
Co	0.130 ± 0.006	0.385 ± 0.027	0.978	0.0025	
Sr	0.060 ± 0.002	0.395 ± 0.016	0.991	0.0003	
Cs	0.277 ± 0.017	0.426 ± 0.031	0.977	0.0167	
Langmuir (Lang) model					
Solute	q_{mL} (mmol g^{-1})	b_L (L mmol^{-1})	R^2	SSE	R_L *
Co	0.312 ± 0.014	0.868 ± 0.148	0.979	0.0024	0.0544
Sr	0.177 ± 0.007	0.501 ± 0.078	0.977	0.0007	0.0906
Cs	0.855 ± 0.068	0.458 ± 0.121	0.958	0.0314	0.0983
Kargi–Ozmihci (K–O) model					
Solute	$q_{m,KO}$ (mmol g^{-1})	b_{KO} (L mmol^{-1})	N_{KO}	R^2	SSE
Co	0.433 ± 0.075	2.108 ± 0.622	0.654 ± 0.087	0.991	0.0011
Sr	0.302 ± 0.042	3.967 ± 0.713	0.592 ± 0.043	0.997	0.0001
Cs	1.965 ± 0.042	5.984 ± 5.285	0.547 ± 0.120	0.980	0.0147
Koble–Corrigan (KC) model					
Solute	$q_{m,KC}$ (mmol g^{-1})	b_{KC} (L mmol^{-1})	N_{KC}	R^2	SSE
Co	0.205 ± 0.026	0.474 ± 0.139	0.654 ± 0.087	0.991	0.0011
Sr	0.076 ± 0.003	0.252 ± 0.045	0.592 ± 0.043	0.997	0.0001
Cs	0.328 ± 0.053	0.167 ± 0.147	0.547 ± 0.120	0.980	0.0147
Langmuir–Freundlich (Lang–Fr) model					
Solute	$q_{m,LF}$ (mmol g^{-1})	b_{LF} (L mmol^{-1})	N_{LF}	R^2	SSE
Co	0.433 ± 0.075	0.474 ± 0.139	0.654 ± 0.087	0.991	0.0011
Sr	0.302 ± 0.042	0.252 ± 0.045	0.592 ± 0.043	0.994	0.0011
Cs	1.965 ± 0.042	0.167 ± 0.147	0.547 ± 0.120	0.990	0.0011

*Calculated at C_0 = 20 mM

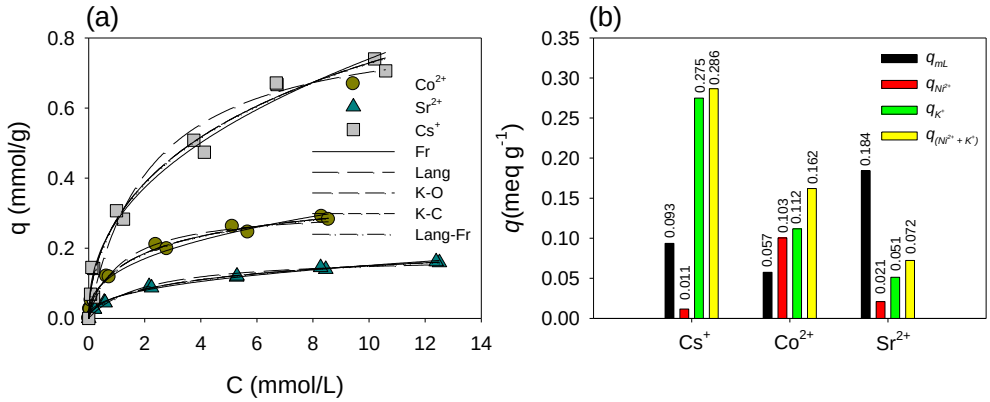

Fig. 6 (a) Single sorption of Co^{2+}, Sr^{2+}, and Cs^{+} onto NM–PAN (lines represent the sorption model predictions) and (b) ion-exchange values of Cs^{+}, Co^{2+}, and Sr^{2+} sorption onto NM–PAN (C_0 = 10 mM)

(q_{K^+}) and Ni^{2+} ($q_{Ni^{2+}}$) in the aqueous solution after the sorption of Co^{2+}, Sr^{2+}, and Cs^{+} at 10 mM. The ion-exchange value for each radioactive element was calculated in the milliequivalent (meq) unit as Co^{2+}, Sr^{2+}, and Cs^{+} have different charges, as shown in Fig. 6b. For monovalent Cs^{+}, the K^{+} ion exchange (q_{K^+} = 0.275 meq g^{-1}) was higher than the Ni^{2+} ion exchange ($q_{Ni^{2+}}$ = 0.011 meq g^{-1}). This was similar for divalent Sr^{2+}, wherein q_{K^+} (0.051 meq g^{-1}) >> $q_{Ni^{2+}}$ (0.021 meq g^{-1}), indicating that the monovalent K^{+} ion exchange (q_{K^+}) was dominant for the sorption of both Cs^{+} and Sr^{2+}. Meanwhile, for divalent Co^{2+}, q_{K^+} (0.112 meq g^{-1}) ≈ $q_{Ni^{2+}}$ (0.103 meq g^{-1}), indicating that the monovalent q_{K^+} and the divalent $q_{Ni^{2+}}$ equally contributed to the sorption. Notably, the $q_{(Ni^{2+}+K^{+})}$ values, representing the total ion

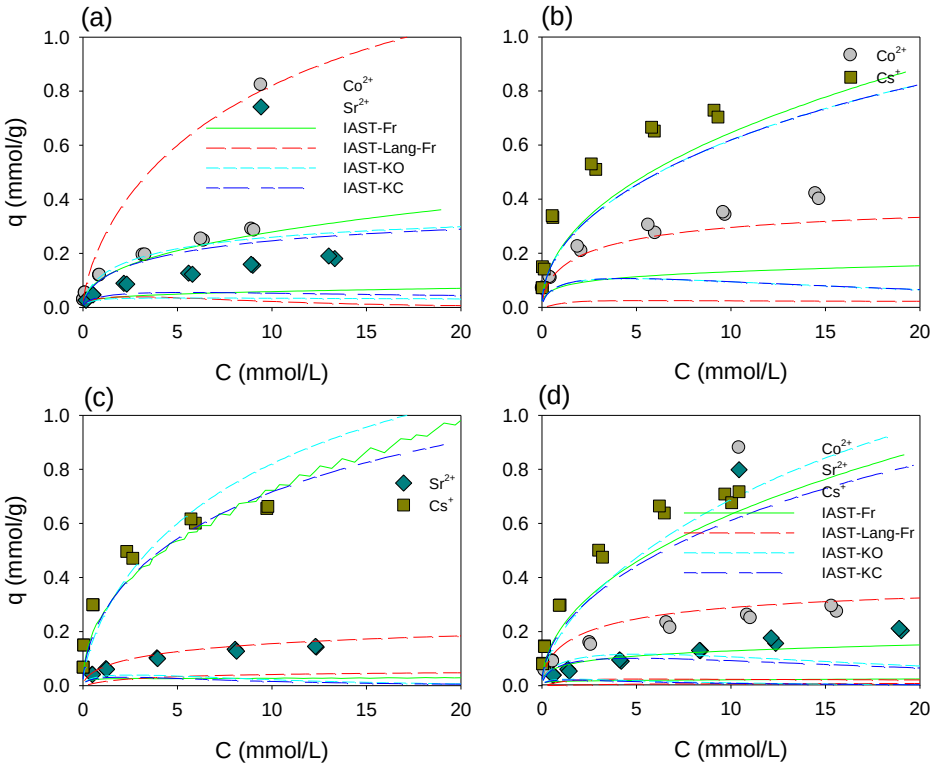

Fig. 7 Bi-solute competitive sorption of (a) Co^{2+}/Sr^{2+}, (b) Co^{2+}/Cs^{+}, (c) Sr^{2+}/Cs^{+}, and (d) tri-solute competitive sorption of $Co^{2+}/Sr^{2+}/Cs^{+}$ onto NM–PAN at pH 5. The lines represent the sorption model predictions

exchange values of KNiFC–PAN for Co^{2+}, Sr^{2+}, and Cs^{+}, respectively, showed a similar order to the q_{mL}, $q_{m,KO}$, $q_{m,KC}$, and $q_{m,LF}$ values: Cs^{+} (0.286 meq g^{-1}) >> Co^{2+} (0.162 meq g^{-1}) > Sr^{2+} (0.072 meq g^{-1}). This result indicated that the q_{mL}, $q_{m,KO}$, $q_{m,KC}$, and $q_{m,LF}$ values are positively correlated with the ion exchange values. The ion exchange reactions for Cs^{+}, Co^{2+}, and Sr^{2+} onto KNiFC–PAN were described below (Eqs. 10-15) (Park *et al.* 2010):

$$Cs^{+} + K^{+}(KNiFC–PAN) \rightarrow K^{+} + Cs^{+}(KNiFC–PAN) \quad (10)$$

$$2Cs^{+} + Ni^{2+}(KNiFC–PAN) \rightarrow Ni^{2+} + 2Cs^{+}(KNiFC–PAN) \quad (11)$$

$$Co^{2+} + 2K^{+}(KNiFC–PAN) \rightarrow 2K^{+} + Co^{2+}(KNiFC–PAN) \quad (12)$$

$$Co^{2+} + Ni^{2+}(KNiFC–PAN) \rightarrow Ni^{2+} + Co^{2+}(KNiFC–PAN) \quad (13)$$

$$Sr^{2+} + 2K^{+}(KNiFC–PAN) \rightarrow 2K^{+} + Sr^{2+}(KNiFC–PAN) \quad (14)$$

$$Sr^{2+} + Ni^{2+}(KNiFC–PAN) \rightarrow Ni^{2+} + Sr^{2+}(KNiFC–PAN) \quad (15)$$

The order pattern of q_{mL}, $q_{m,KO}$, $q_{m,KC}$, and $q_{m,LF}$ values (Cs^{+} >> Co^{2+} > Sr^{2+}) in this study can be explained by the radii of hydrated ions, wherein the ion radius expands through the ion-water interaction (Nightingale, 1959). According to Nightingale (1959) the Co^{2+}, Sr^{2+}, and Cs^{+} radii after hydration were in the following order: Cs^{+} (3.29 Å) << Sr^{2+} (4.12 Å) < Co^{2+} (4.23 Å), whereas the pore size of NM–PAN was considerably larger (55.19 Å, Table 1) than those of hydrated Cs^{+}, Sr^{2+}, and Co^{2+} ions. As expected, the Cs^{+} sorption capacity was much higher than those of Co^{2+} and Sr^{2+} (Table 3) when the radius of the hydrated Cs^{+} ion was smaller than the sorbent's pore size (55.19 Å), leading to the higher sorption capacity of the Cs^{+} ion onto the sorbent. The R_L values indicated that the sorption of Co^{2+}, Sr^{2+}, and Cs^{+} onto NM–PAN was favorable ($0 < R_L < 1$, Table 3). Overall, the Cs^{+}, Co^{2+}, and Sr^{2+} sorptions onto NM–PAN was dominated by the physical sorption through ion exchange mechanism, whereas the Cs^{+} affinity towards the NM–PAN was higher than the affinities of Co^{2+}, and Sr^{2+}.

3.4 Sorption in binary and ternary systems

The binary sorption data were fitted by the IAST model coupled with the single sorption models of IAST–Fr, IAST–Lang–Fr, IAST–KO and IAST–KC, as shown in Fig. (7a–c). The model parameters of bi-solute competitive sorptions of Co^{2+}/Sr^{2+} (Fig. 7a), Co^{2+}/Cs^{+} (Fig. 7b), and Sr^{2+}/Cs^{+} (Fig. 7c) onto NM–PAN were presented in Table 4. As indicated by R^2 values (> 0.909), the Fr model fitted well to the all bi-solute competitive systems. The IAST–Fr model showed the best fitting result (0.0033 < SSE < 0.3407, 0.0191 < RMSE < 0.1946) compared to the IAST–Lang–Fr (0.0021 < SSE < 2.5257, 0.0152 < RMSE <

Table 4 R^2 and SSE values for the predictions of bi-solute competitive sorption of Co^{2+}, Sr^{2+} and Cs^{+} onto NM–PAN at pH 5

Support	Solute	R^2	SSE	RMSE
IAST–Fr	Co^{2+}/Sr^{2+}	0.991/0.909	0.0033/0.0666	0.0191/0.0860
	Sr^{2+}/Cs^{2+}	0.932/0.972	0.0608/0.0637	0.0932/0.0841
	Co^{2+}/Cs^{+}	0.909/0.925	0.3407/0.2027	0.1946/0.1501
IAST–Lang–Fr	Co^{2+}/Sr^{2+}	0.994/0.074	0.0021/0.1576	0.0152/0.1323
	Sr^{2+}/Cs^{2+}	0.980/0.104	0.0021/2.0698	0.0174/0.4796
	Co^{2+}/Cs^{+}	0.959/0.069	0.0350/2.5257	0.0623/0.5298
IAST–KO	Co^{2+}/Sr^{2+}	0.988/0.410	0.0047/0.1004	0.0228/0.1056
	Sr^{2+}/Cs^{2+}	0.400/0.942	0.0642/0.1326	0.0958/0.1214
	Co^{2+}/Cs^{+}	0.477/0.913	0.4556/0.2361	0.2250/0.1620
IAST–KC	Co^{2+}/Sr^{2+}	0.975/0.578	0.0099/0.0719	0.0332/0.0894
	Sr^{2+}/Cs^{2+}	0.312/0.966	0.0736/0.0772	0.1025/0.0926
	Co^{2+}/Cs^{+}	0.477/0.917	0.4556/0.2238	0.2250/0.1577

Table 5 R^2 and SSE values for the predictions of tri-solute competitive sorption of Co^{2+}, Sr^{2+} and Cs^{+} onto NM–PAN at pH 5

Model	R^2	SSE	RMSE
IAST–Fr	0.874/0.867/0.781	0.1043/0.1480/0.5507	0.1077/0.1281/0.1103
IAST–Lang–Fr	0.945/0.088/0.078	0.0253/0.1840/2.3218	0.0407/0.1436/0.5093
IAST–KO	0.676/0.118/0.958	0.1492/0.1780/0.1051	0.1307/0.1393/0.1094
IAST–KC	0.618/0.101/0.948	0.1763/0.1820/0.1299	0.1423/0.1410/0.1239

0.5297), IAST–KO (0.0047 < SSE < 0.4556, 0.0228 < RMSE < 0.225) and IAST–KC (0.0099< SSE < 0.4556, 0.0332 < RMSE < 0.225) models. In the bi-solute systems, the interactions between two solutes may mutually enhance (synergism) or inhabit (antagonism) the sorption capacity, or no interaction occurs (Aksu and Akpinar, 2001). This is caused by some complicated reasons such as the characteristics of the binding sites (e.g., functional groups, structure, surface properties etc.), the properties of the sorbates (e.g., concentration, ionic size, ionic weight, molecular structure, ionic nature, or standard reduction potential etc.) and solution chemistry (e.g., pH, ionic strength, etc.) (Oh *et al.* 2015). The tri-solute competitive sorption data of $Co^{2+}/Sr^{2+}/Cs^{+}$ onto NM–PAN were fitted to the multi-solute sorption models (Fig. 7d). The model parameters of IAST–Fr, IAST–Fr–Lang, IAST–K–O, and IAST–K–C were summarized in Table 5. According to the R^2 values, IAST–Fr (> 0.781) model prediction was in good agreement with experimental data, whereas IAST–Lang–Fr, IAST–K–O, and IAST–K–C were not satisfactory.

3.5 Effect of surfactants

Different types of surfactants are utilized in the detergents used to clean the human body, household appliances, and protective clothing. Therefore, it is important to investigate various surfactants (Table S1) that can affect the sorption of radioactive elements onto NM–PAN. The effects of surfactants on the sorption of Co^{2+}, Sr^{2+}, and Cs^{+} onto NM–PAN were evaluated by the K_d value and compared to those without the use of surfactants (i.e., control experiment), as shown in Fig. 8.

Sorption behaviors of Co^{2+}, Sr^{2+} and Cs^{+} onto NM–PAN in the presence of three different types of surfactants were widely different. For non-ionic surfactants, the K_d values of both Triton X-100 (Fig. 8a) and Tween-80 (Fig. 8b) slightly increased the sorption of Co^{2+} and Cs^{+} onto NM–PAN, but slightly decreased that of Sr^{2+}. As the concentration of cationic surfactants, OTMA and HDTMA increased to near CMC, the K_d values of Co^{2+} and Cs^{+} increased but that of Sr^{2+} decreased (Fig. 8c, d).

For the cationic surfactants OTMA (Fig. 8c) and HDTMA (Fig. 8d), below CMC did not significantly affect the K_d val1ues of Co^{2+} and Cs^{+}, whereas near CMC highly affected the K_d values of Co^{2+} and Cs^{+}. The cationic surfactant OTMA was effective in reducing the repulsion force only when it was near its CMC, whereas the non-ionic surfactants did not affect the repulsion force and thus had no effect on the K_d values.

The presence of anionic surfactant, SOBS highly affected the sorption of Co^{2+}, Sr^{2+} and Cs^{+} onto NM–PAN (Fig. 8e). When SOBS was present in the metal solutions, the sorption's of Co^{2+}, Sr^{2+} and Cs^{+} sharply increased. in the presence of SDBS, the K_d value of Co^{2+} was increased at blow CMC but decreased at near CMC, but that of Sr^{2+} hardly changed. However, The K_d value of Cs^{+} increased as SDBS concentration increased (Fig. 8f). Anionic surfactant molecules, which are negatively charged, can bind with positively charged metal ions and thus the formation of

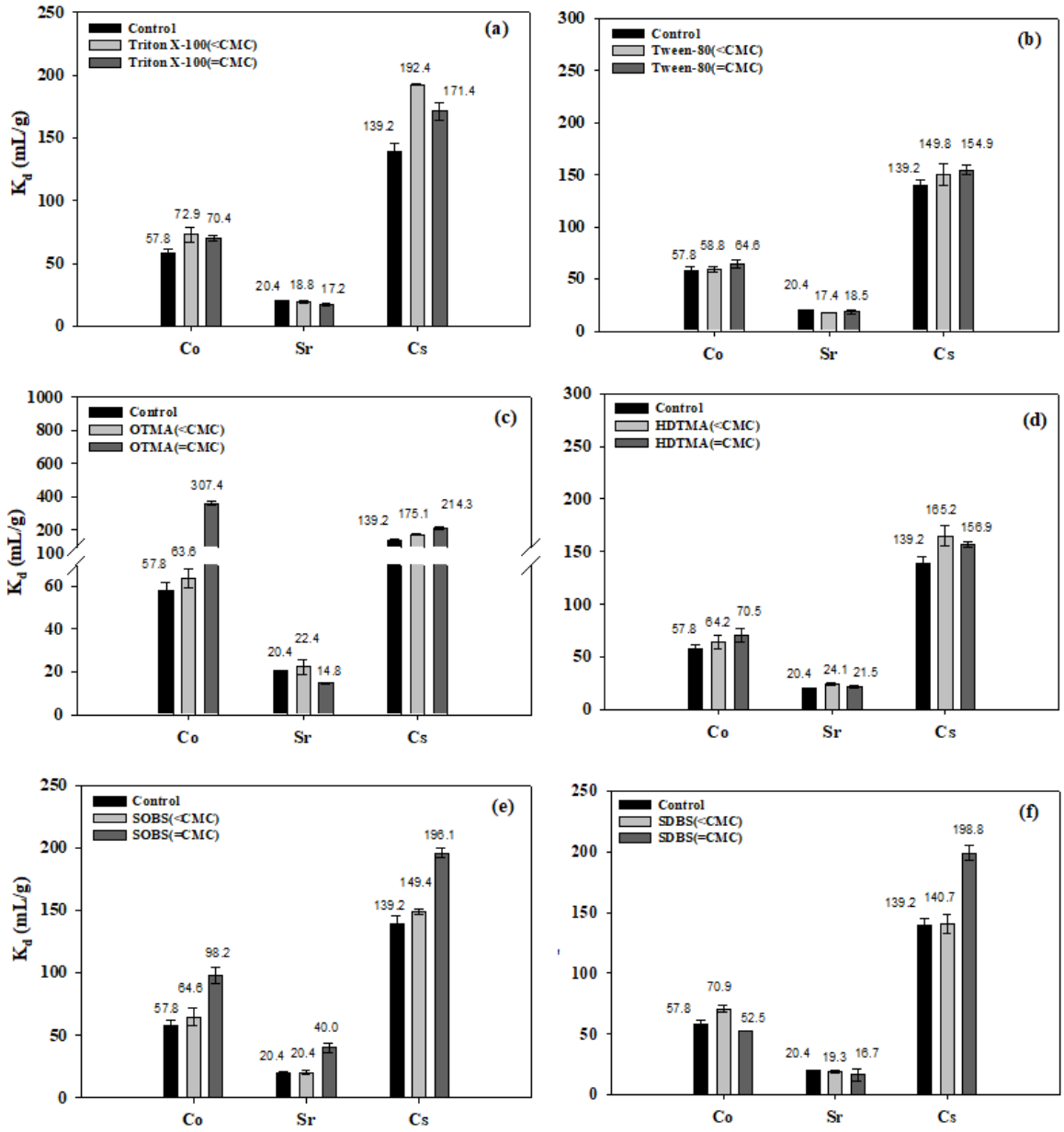

Fig. 8 Effect of surfactants on the distribution coefficients (K_d) of Co^{2+}, Sr^{2+}, and Cs^{+} using (a) Triton X-100, and (b) Tween-80, (c) OTMA, (d) HDTMA, (e) SOBS, and (f) SDBS. Co^{2+}/ Sr^{2+}/Cs^{+} = 10 mM, V/m = 30 mL g^{-1} for Co^{2+} and Sr^{2+}, and 75 mL g^{-1} for Cs^{+}), experimental time = 24 h at 25°C

cation-SDBS or -SOBS complex can occur in the solution (Li and Bowman 1997). When SDBS was present in Co^{2+} solution, the sorption of Co^{2+} on the accessible sorption sites of NM–PAN surfaces may be inhibited due to the formation of Co-SDBS complex.

4. Conclusions

An NM–PAN composite was synthesized as a sorbent for the single, binary, and ternary sorption of Co^{2+}, Sr^{2+}, and Cs^{+} from radioactive laundry wastewater. The NM–PAN composite can be used as a typical sorbent for removing radioactive waste from wastewater. The Fr, Lang, K–O, K–C, and Lang–Fr models satisfactorily predicted all the single sorption data. In this study, the sorption isotherms were nonlinear. Among the three radioactive elements in laundry wastewater, Cs^{+} showed a higher maximum sorption capacity than Co^{2+} and Sr^{2+}. The sorption capacities of Co^{2+}, Sr^{2+}, and Cs^{+} in the single system were less than those in the binary and ternary systems. Among all competitive sorption models, such as the IAST–Fr, IAST–Lang, and IAST–Lang–Fr models, the IAST–Fr, showed the most satisfactory prediction for the binary and ternary systems. Among the three types of surfactants, the anionic surfactants (SOBS and SDBS) and anionic surfactants (OTMA) affected the sorption processes by reducing the repulsion forces. The results of this study show that the IAST–Fr, IAST–Lang, and IAST–Lang–Fr models can be used to predict the binary and ternary sorption of radioactive waste elements onto NM–PAN.

Acknowledgments

This work was supported by Korea Environmental Industry & Technology Institute (KEITI) through Aquatic Ecosystem Conservation Research Program, funded by Korea Ministry of Environment (MOE) (No. 202100304 0004).

References

Aksu, Z. and Akpinar, D. (2001), "Competitive biosorption of phenol and chromium(VI) from binary mixtures onto dried anaerobic activated sludge", *Biochem. Eng. J.*, **7**(3), 183-193. https://doi.org/10.1016/S1369-703X(00)00126-1.

Babatunde, A.O., Zhao, Y.Q. (2010), "Equilibrium and kinetic analysis of phosphorus adsorption from aqueous solution using waste alum sludge", *J. Hazard. Mater*. **184**, 746-752. https://doi.org/10.1016/j.jhazmat.2010.08.102.

Ebner, A.D., Ritter, J.A. and Navratil, J.D. (2001), "Adsorption of cesium, strontium, and cobalt ions on magnetite and a magnetite−silica composite", *Ind. Eng. Chem. Res.*, **40**(7), 1615-1623. https://doi.org/10.1021/ie000695c.

Eren, E., Afsin, B. and Onal, Y. (2009), "Removal of lead ions by acid activated and manganese oxide-coated bentonite", *J. Hazard. Mater.*, **161**(2-3), 677-685. https://doi.org/10.1016/j.jhazmat.2008.04.020.

Gonzalez de Vicente, S.M., Smith, N.A., El-Guebaly, L., Ciattaglia, S., Di Pace, L., Gilbert, M., Mandoki, R., Rosanvallon, S., Someya, Y., Tobita, K., Torcy, D. (2022), "Overview on the management of radioactive waste from fusion facilities: ITER, demonstration machines and power plants", *Nucl. Fusion*, **62**, 085001. https://doi.org/10.1088/1741-4326/ac62f7.

Granados Correa, F. and Jiménez-Becerril, J. (2004), "Adsorption of 60 Co^{2+} on hydrous manganese oxide powder from aqueous solution", *Radiochim. Acta*, **92**(2), 105-110. https://doi.org/10.1524/ract.92.2.105.27459.

Ismail, I.M., El-Sourougy, M.R., Moneim, N.A. and Aly, H.F. (1999), "Equilibrium and kinetic studies of the sorption of cesium by potassium nickel hexacyanoferrate complex", *J. Radioanal. Nucl. Chem.*, **240**, 59-67. https://doi.org/10.1007/BF02349137.

Kadadou, D., Said, E.A., Ajaj, R. and Hasan, S.W. (2023), "Research advances in nuclear wastewater treatment using conventional and hybrid technologies: Towards sustainable wastewater reuse and recovery", *J. Water Process Eng.*, **52**, 103604. https://doi.org/10.1016/j.jwpe.2023.103604.

Kargi, F. and Ozmıhcı, S. (2004), "Biosorption performance of powdered activated sludge for removal of different dyestuffs", *Enzyme Microb. Technol.*, **35**(2-3). 267-271. https://doi.org/10.1016/j.enzmictec.2004.05.002.

Le, Q.T.N. and Cho, K. (2021), "Cesium adsorption on a zeolitic imidazolate framework (ZIF-8) functionalized by ferrocyanide", *J. Colloid Interface Sci.*, **581**, 741-750. https://doi.org/10.1016/j.jcis.2020.08.017.

Lee, R., Jho, E.H., An, J. (2023). "Sorption of Pb and Cu on different types of microplastics", *Membr. Water Treat.*, **14**(1), 19-25. https://doi.org/10.12989/mwt.2023.14.1.019.

Li, Z. and Bowman, R.S. (1997), "Counterion effects on the sorption of cationic surfactant and chromate on natural clinoptilolite", *Environ. Sci. Technol.*, **31**(8), 2407-2412. https://doi.org/10.1021/es9610693.

Liu, H., Tong, L., Su, M., Chen, D., Song, G. and Zhou, Y. (2023), "The latest research trends in the removal of cesium from radioactive wastewater: A review based on data-driven and visual analysis", *Sci. Total Environ.*, **869**, 161664. https://doi.org/10.1016/j.scitotenv.2023.161664.

Ma, B., Shin, W.S., Oh, S., Park, Y.-J. and Choi, S.-J. (2010), "Adsorptive removal of Co and Sr ions from aqueous solution by synthetic hydroxyapatite nanoparticles", *Sep. Sci. Technol.*, **45**(4), 453-462. https://doi.org/10.1080/01496390903484941.

Masud, M.A.A., Annamalai, S. and Shin, W.S. (2023a), "Remediation of ciprofloxacin in soil using peroxymonosulfate activated by ball-milled seaweed kelp biochar: Performance, mechanism, and phytotoxicity", *Chem. Eng. J.*, **465**, 142908. https://doi.org/10.1016/j.cej.2023.142908.

Masud, M.A.A., Shin, W.S. and Kim, D.G. (2023b), "Fe-doped kelp biochar-assisted peroxymonosulfate activation for ciprofloxacin degradation: Multiple active site-triggered radical and non-radical mechanisms", *Chem. Eng. J.*, **471**, 144519. https://doi.org/10.1016/j.cej.2023.144519.

Masud, M.A.A. and Shin, W.S. (2022), "Single and binary competitive sorption of phenanthrene and pyrene in natural and synthetic sorbents", *J. Soil Groundwater Environ.*, **27**(6), 11-21. https://doi.org/10.7857/JSGE.2022.27.6.011.

Masud, M.A.A., Choi, J. and Shin, W.S. (2022), "Identification of tetrachloroethylene sorption behaviors in natural sorbents via sorption models", *J. Soil Groundwater Environ.*, **27**(6), 47-57. https://doi.org/doi.org/10.7857/JSGE.2022.27.6.047.

Min, K.J., An, H.J., Lee, A.H., Shin, H.G., Park, K.Y. (2023). "Electrodialysis with a channeled stack for high strength cadmium removal from wastewater", *Membr. Water Treat*., **14**(1), 47-54. https://doi.org/10.12989/mwt.2023.14.1.047

Moon, J.K., Kim, K.W., Jung, C.H., Shul, Y.G. and Lee, E.H. (2000), "Preparation of organic-inorganic composite adsorbent beads for removal of radionuclides and heavy metal ions", *J. Radioanal. Nucl. Chem.*, **246**, 299-307. https://doi.org/10.1023/A:1006714322455.

Nightingale, E.R. (1959), "Phenomenological theory of ion solvation. effective radii of hydrated ions", *J. Phys. Chem.*, **63**(9), 1381-1387. https://doi.org/10.1021/j150579a011.

Nilchi, A., Saberi, R., Moradi, M., Azizpour, H. and Zarghami, R. (2011), "Adsorption of cesium on copper hexacyanoferrate-PAN composite ion exchanger from aqueous solution", *Chem. Eng. J.*, **172**(1), 572-580. https://doi.org/10.1016/j.cej.2011.06.011.

Oh, S., Shin, W.S. and Choi, S.J. (2015), "Hydrous manganese oxide-polyacrylonitrile (HMO-PAN) composite for the treatment of radioactive laundry wastewater", *J. Radioanal. Nucl. Chem.*, **303**, 495-508. https://doi.org/10.1007/s10967-014-3583-2.

Park, Y., Lee, Y.C., Shin, W.S. and Choi, S.J. (2010), "Removal of cobalt, strontium and cesium from radioactive laundry wastewater by ammonium molybdophosphate-polyacrylonitrile (AMP-PAN)", *Chem. Eng. J.*, **162**(2), 685-695. https://doi.org/10.1016/j.cej.2010.06.026.

Park, Y., Shin, W.S. and Choi, S.-J. (2013), "Removal of cobalt and strontium from groundwater by sorption onto fishbone", *J. Radioanal. Nucl. Chem.*, **295**, 789-799. https://doi.org/10.1007/s10967-012-1959-8.

Radke, C.J. and Prausnitz, J.M., (1972), "Thermodynamics of multi-solute adsorption from dilute liquid solutions. *AIChE J.*, **18**(4), 761-768. https://doi.org/10.1002/aic.690180417.

Rauwel, P. and Rauwel, E. (2019), "Towards the extraction of radioactive cesium-137 from water via graphene/CNT and nanostructured prussian blue hybrid nanocomposites: A review", *Nanomaterials*, **9**(5), 682. https://doi.org/10.3390/nano9050682.

Rumynin, V.G. and Nikulenkov, A.M. (2016), "Geological and physicochemical controls of the spatial distribution of partition coefficients for radionuclides (Sr-90, Cs-137, Co-60, Pu-239, 240 and Am-241) at a site of nuclear reactors and radioactive waste disposal (St. Petersburg region, Russian Federation) ", *J.*

Environ. Radioact., **162-163**, 205-218. https://doi.org/10.1016/j.jenvrad.2016.05.030.

Sopapan, P., Lamdab, U., Akharawutchayanon, T., Issarapanacheewin, S., Yubonmhat, K., Silpradit, W., Katekaew, W. and Prasertchiewchan, N. (2023), "Effective removal of non-radioactive and radioactive cesium from wastewater generated by washing treatment of contaminated steel ash", *Nucl. Eng. Technol.*, **55**(2), 516-522. https://doi.org/10.1016/j.net.2022.10.007.

YH